Biomimetic Synthesis and Characterization of Hydroxyapatite Crystal with Low Phase Transformation Temperature

Hongshi Zhao,[†] Wen He,*[,†,‡] Yingjun Wang,[‡] Xudong Zhang,[†] Zhengmao Li,[†] Shunpu Yan,[†] and Weijia Zhou[†]

Department of Materials Science and Engineering, Shandong Institute of Light Industry, Jinan 250353, P. R. China, and Biomaterials Research Center, South China University of Technology, Guangzhou 510640, P. R. China

Hydroxyapatite (HA) with a low phase transformation temperature was synthesized via a biomimetic route using ovalbumin as a natural biosurfactant. The resulting materials were characterized by means of X-ray diffraction (XRD), differential thermal analysis (DTA), Fourier transform infrared spectroscopy (FTIR), and transmission electron microscopy (TEM). The results show that needle-like HA nanocrystals can be obtained at room temperature. The HA crystals can transform to β-tricalcium phosphate (β-TCP) nanocrystals as low as about 550 °C. Furthermore, it is proved using the electrophoretic method that there are superfluous positive charges on the surface of the HA particles. The substitution of PO_4^{3-} ions by CO_3^{2-} ions in the HA crystal is the predominant factor in affecting the low phase transformation and the surface electrical charges of the particles. A schematic illustration was used to depict the protein-medicated crystallization of HA crystals with positive charges.

1. Introduction

The hard tissue of vertebrates is mainly composed of nonstoichiometric hydroxyapatite ($Ca_{10}(PO_4)_6(OH)_2$, HA) and collagen.[1] Collagen is the most commonly utilized protein to form life on earth. Studies on HA/collagen composites are reported widely, and most of the artificial biomimetic HA/collagen composites are similar with natural bone tissue both in structure and in composition.[2,3] Recently, macromolecules, as controllers of mineral nucleation and growth for the synthesis of mineral−polymer composite biomaterials, have generated considerable interest, [4] especially the bioorganic materials, i.e., chitosan,[5] silk protein,[6] and bacterial cellulose[7] due to their bioactivity, biocompatibility, and nontoxicity. Previous researchers have stated that macromolecules can form biological matrices containing acidic macromolecules rich in negatively charged groups, which will control the nucleation, growth, orientation, and chemical composition of crystals.[8] The protein molecules have various charged groups, i.e., carboxyl, amido, phosphatic, and hydroxyl. In the presence of calcium and phosphate ions, the protein can lead to controlled HA growth, and thus it has become one of the most promising biosurfactants in the preparation of apatite crystals. However, the proteins previously used are expensive and difficult to extract from organisms, and even the most promising collagen is difficult to define due to its diversity. In contrast, ovalbumin extracted from egg white is a very stable protein in structure, which is biocompatible, is abundant in source, has a low production cost, and can be modified to gain a variety of chemical, physical, and biological properties.[9] It is widely used in the food industry due to its high content of nutritious protein. In view of this, we used ovalbumin as a natural biosurfactant to synthesize HA crystals at room temperature, while the conventional synthetic routes need additional power such as microwave power, thermal treatment, or hydrothermal conditions.[10,11] Compared with the phase and thermal stability of nanocrystalline HA synthesized by other methods,[12,13] the HA crystals obtained with this method can transform to β-tricalcium phosphate (β-TCP) crystals at temperatures as low as about 550 °C.

This paper reports on the synthesis and characterization of HA crystals with a low phase transformation temperature using a biomimetic method. Further studies on the mechanism of the low phase transformation temperature of HA to β-TCP will be summarized in our next study.

2. Experimental Sections

Materials. The ovalbumin without further purification was directly extracted from egg white consisting of water [(85 to 88) wt %] and protein [(11 to 13) wt %].[9] Diammonium hydrogen phosphate was purchased from the Tianjin Baishi Chemical and Industry Ltd. Calcium nitrate tetrahydrate was purchased from Bodi Chemical and Industry Ltd. All the reagents used were analytical grade.

Synthesis. The composite was prepared by the precipitation method. First, 5 g of ovalbumin was added to 20 mL of distilled water with gentle stirring for 0.5 h, and then 0.6 M $(NH_4)_2HPO_4$ was added to the ovalbumin solution with strong stirring for another 0.5 h while the pH value of the solution was adjusted at 8.5 with ammonia (12.5 wt %). Then, 0.4 M calcium nitrate tetrahydrate was added dropwise to the surfactant/phosphorus solution with continuous stirring for 1 h, while the pH value was kept at 8.5 during the addition. The final Ca/P ratio was maintained at 1.67, and the suspension was sealed at room temperature for 3 days. Finally, the precipitate was collected and washed twice with deionized water and once with ethanol, followed by drying at 80 °C for 24 h. The sample uncalcined was designated as FB0, while the samples calcined at (300, 500, and 700) °C were designated as FB3, FB5, and FB7, respectively.

Characterization Procedures. Wide-angle (10° to 90°) X-ray powder diffraction (XRD) patterns were obtained using a PANalytical X'Pert PRO X-ray diffractometer with Cu Kα (λ

* Corresponding author. Tel.: +86 531 8984 5274. Fax: +86 531 8861 9798. E-mail address: hewen1960@126.com.
[†] Shandong Institute of Light Industry.
[‡] South China University of Technology.

10.1021/je800058d CCC: $40.75 © 2008 American Chemical Society
Published on Web 11/16/2008

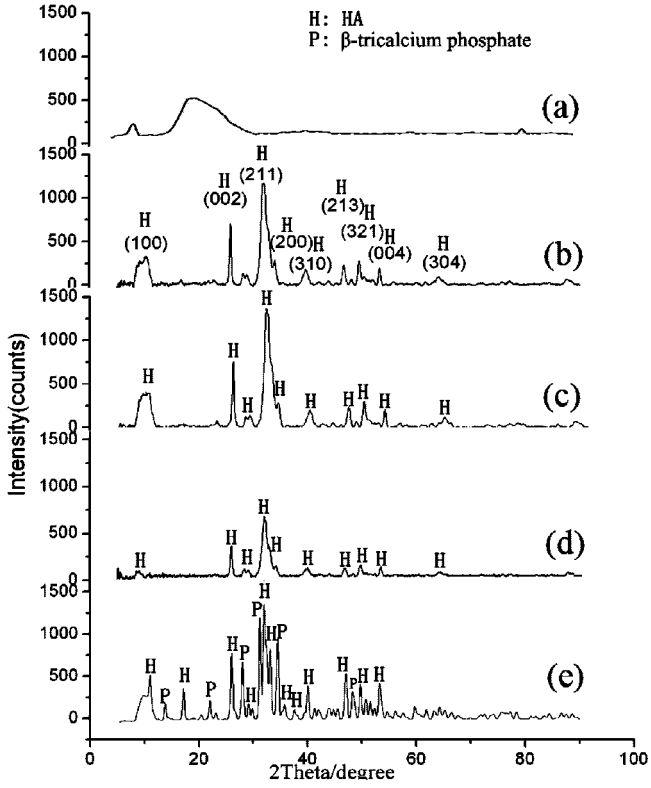

Figure 1. Wide angle XRD patterns of the dry ovalbumin powder and the samples calcined at different temperatures: (a) dry ovalbumin powder, (b) FB0, (c) FB3, (d) FB5, (e) FB7.

= 0.15418 nm) incident radiation. The powders were investigated using Fourier transform infrared (FTIR) spectroscopy ([FTIR] NEXUS 470, Nicolet, USA). The morphology of the products was studied by transmission electron microscopy (TEM), carried out on a TEM-100X electron microscope. The Brunauer−Emmett−Teller (BET) surface areas of the powders were analyzed by nitrogen adsorption in a Micromeritics ASAP 2000 nitrogen adsorption apparatus. The surface charge of the particles was characterized by JS94H microelectrophoresis (Powereach, Shanhai, China) and the conductometer model DDS-11A (Shanghai Leici Corporation, China).

3. Results and Discussion

3.1. XRD Analysis. The XRD patterns of the samples obtained in this work are shown in Figure 1. The broad peak shows that the dry ovalbumin powder is noncrystalline (Figure 1a). As seen from Figure 1(b, c), all the XRD peaks can be *hkl* indexed based on a hexagonal HA crystal of space group $P6_3/m$ ($a = b = 9.418$ Å, $c = 6.884$ Å) with reference to the standard Powder Diffraction File (PDF Card no. 09-432). It shows that good HA crystals can be obtained at low temperatures (Figure 1b, c), while the intensity of the reflection peaks is weakened sharply by increasing the temperature to 500 °C (Figure 1d) and some weak peaks disappear, indicating structural transformation of the nanocrystals. After heat treatment at 700 °C, the new phase can be clearly identified as β-tricalcium phosphate (β-TCP) (PDF Card no. 09-0169) (Figure 1e). According to the accepted formula (eq 1),[14] the content of HA is calculated to be 81.5 % and β-TCP at 18.5 %.

$$y = 1 - \frac{1}{1 + 3.9\frac{I_a}{I_c}} \quad (1)$$

In the equation, y is the mass fraction of HA in the HA/β-TCP polycrystal, and I_a and I_c are the intensities of the (211) reflection peak of HA and the (0, 2, 10) reflection peak of β-TCP, respectively. Table 1 shows the parameter changes of HA crystals calcined at different temperatures, and FB5 shows the biggest crystal lattice distortion which indicates crystal transformation.

3.2. DTA Analysis. Thermal analysis is an important analytical method in understanding the structure−property relationship of the inorganic reinforced polymeric composites. Moreover, it is a useful technique to determine the thermal stability of the materials.[15,16] Figure 2(a, b) shows DTA curves of dry ovalbumin powders and FB0. It can be seen from Figure 2a that an endothermic peak at 134 °C is due to desorption of water and the thermal decomposition of partial organic substances, and a broad exothermic peak at 276 °C is ascribed to the decomposition and combustion of ovalbumin (Figure 2a). The DTA curve relative to the composite FB0 is shown in Figure 2b, which demonstrates the interaction of the inorganic phase with protein molecules and the crystal transformation of HA to β-TCP. The DTA results strongly support the existence of organic materials in the composite as high as 500 °C. The broad exothermic peak between (270 and 558) °C is caused by the combustion of the organic materials combined with HA nanocrystals (Figure 2b). [17] The plot appears modified if compared with those of pure dry ovalbumin powders, demonstrating the interaction of the inorganic phase with protein molecules. An even rise between (558 and 900) °C can be observed in DTA curve (b), and according to the XRD and FTIR analysis (Figure 1d,e and Figure 3c,d), it is not caused by the combustion of the organic materials but the phase transformation of HA to β-TCP. It can be deduced that HA will be converted into β-TCP completely at any temperature between (558 and 700) °C if given enough heat preservation time.

3.3. FT-IR Spectra. Both HA crystals calcined at different temperatures and dry ovalbumin powders were further investigated using Fourier transform infrared (FTIR) spectroscopy as shown in Figure 3. In Figure 3a, the bands at 563 cm^{-1}, 601 cm^{-1}, and 1035 cm^{-1} can be ascribed to PO_4^{3-} ions, at 1456 cm^{-1} to CO_3^{2-} ions, and at 3560 cm^{-1} to OH^- ions. The broadband at (3500 to 3300) cm^{-1} is ascribed to the nitrogen−hydrogen stretches (N−H), and the bands at 2927 cm^{-1}, 1654 cm^{-1}, and 1540 cm^{-1} are ascribed to carbon−hydrogen vibration (C−H), the carbonyl vibration (C═O), and the stretching vibrations of carbon−nitrogen (C−N). It is seen in the spectrum (e) that the corresponding bands are at (3300 to 3500) cm^{-1}, 2974 cm^{-1}, 1664 cm^{-1}, and 1559 cm^{-1}, which have wavenumbers similar with spectrum (a). Comparing Figure 3a with (b), (c), and (d), the intensity of these bands becomes lower and lower with the increase of the calcining heat, while at 700 °C, those bands disappear (Figure 3d). Therefore, large amounts of residual ovalbumin are in FB0 and FB3. The carbonate groups from air that are not removed completely with calcining heat as high as 500 °C have stronger combination with HA crystals than other groups. The CO_3^{2-} groups may substitute some PO_4^{3-} groups, which lead to the reduction of negative charges and the lattice distortion of the HA crystal, and thus decrease the crystal transition energy.

The magnification parts of the spectra below 1000 cm^{-1} are shown in Figure 3 (see the inset). The FTIR spectra of the samples can be used to calculate the crystallinity index (CI) (so-called splitting factor, SF), defined as the sum of the absorbance at ~565 cm^{-1} and ~605 cm^{-1} divided by the absorbance at ~595 cm^{-1}.[18,19] The SF is a measure of the crystal size and the degree of the crystal lattice order. Consequently, large apatite crystals with better atomic order show stronger expressed separation between the absorption peaks at 563 cm^{-1} and 603 cm^{-1}. The splitting peak was measured by

Table 1. Parameter Changes of HA Crystals Calcined at Different Temperatures

	lattice constants			fwhm[a](002)	crystallite size	crystallinity	crystal lattice distortion
specimen	*a*	*b*	*c*	(rad)	(nm)	(X_c)	(*e*)
FB0	9.413	9.413	6.844	0.0079	18.01	0.147	0.0087
FB3	9.428	9.428	6.884	0.0076	18.73	0.166	0.0083
FB5	9.436	9.436	6.896	0.0088	16.18	0.109	0.0096
FB7	9.419	9.419	6.883	0.0075	19.00	0.173	0.008

[a] fwhm: full-width at half-maximum of peak height.

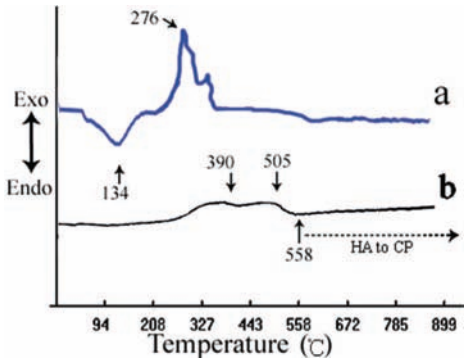

Figure 2. DTA curves of the dry ovalbumin powder (a) and FB0 (b).

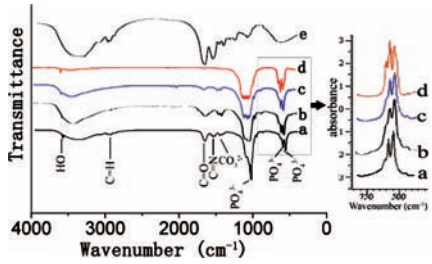

Figure 3. FTIR spectra of the samples: (a) FB0, (b) FB3, (c) FB5 (d) FB7, (e) dry ovalbumin powder.

Table 2. BET Surface Areas of the Samples Calcined at Different Temperaments

specimen	FB0	FB3	FB5	FB7
BET ($m^2 \cdot g^{-1}$)	53	117	98	8.3

the KnowItAll (R) 5.0 software (Bio-Rad Laboratories, USA). The higher the SF value, the better the crystallinity. The SF values of FB0, FB3, FB5, and FB7 are calculated to be 3.78, 3.92, 3.17, and 3.81, respectively. The conclusions obtained from the SF are similar to the XRD analysis.

3.4. BET Analysis and TEM Observation. The BET surface areas of the samples calcined at different temperatures are summarized in Table 2. It shows that the surface area of FB3 with a crystallite size at 18 nm reaches a maximum of 117 $m^2 \cdot g^{-1}$, while FB5 sized at 16 nm just shows a BET value of 98 $m^2 \cdot g^{-1}$ because of the agglomeration of the crystallites during calcination. The surface area of FB3 is larger than FB0 due to the existence of pores after the removal of organic materials. On calcining at 700 °C, the BET value decreases markedly to 8.3 $m^2 \cdot g^{-1}$, while the particle size increases to (100 to 200) nm in width due to the aggregation of crystallites sized at 19 nm (Figure 4g). The serious agglomeration is ascribed to the removal of the organic materials, indicating that the protein can be used not only as a template to control the crystal growth but also as a dispersant to avoid the agglomeration of the crystal grains.

The TEM images are taken to judge the morphology changes of the samples calcined at different temperatures. Figure 4a shows that the whole particle is composed of many small needle-like particles. The small particles are connected with each other by organic materials and distributed randomly in a network structure. Due to the high content of the organic materials, the images seem to be a little blurred (Figure 4a, b). When calcined at 300 °C for 3 h, the needle-like particles begin to aggregate together by the physical attractions of the elemental nanocrystals. After being calcined at 500 °C for 3 h, most of the organic matter is removed, and the HA nanocrystals aggregate to form rodlike particles (Figure 4c). Figure 4d shows that large particles can be obtained which keep connecting with each other end to end, and they are measured at a submicron scale. Compared with the crystallite size calculated by Scherrer's equation, the large particles are aggregated by crystallites sized at about 19

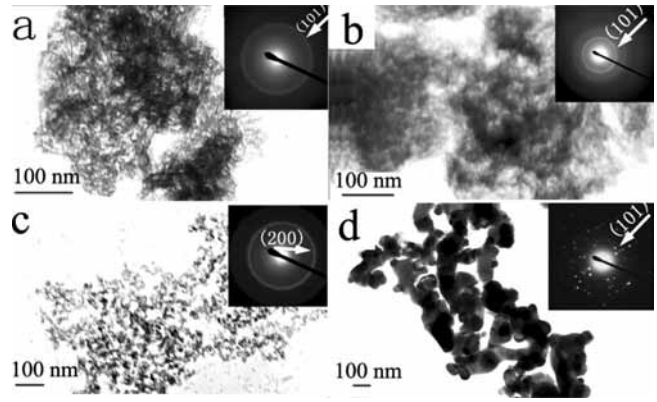

Figure 4. Influence of calcining heat on microstructural features of nanopowders exhibited from TEM and (inset) the electron diffraction patterns: (a) FB0, (b) FB3, (c) FB5, (d) FB7.

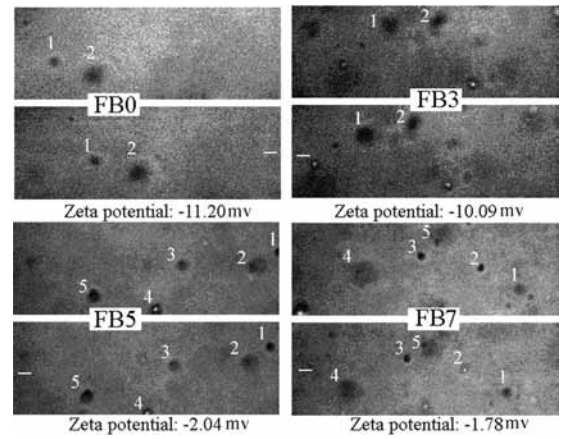

Figure 5. Electrophoregrams of the powders dispersed in distilled water. Arabic numerals represent the moving direction of the same particles. The white bars represent the negative polarity of the instantaneous voltage.

Table 3. Electrical Conductivity of the Powders Dispersed in Distilled Water (a) and 0.033 M Sodium Hydroxide Solution (b), Respectively

specimen	FB0	FB3	FB5	FB7
a ($\mu S \cdot cm^{-1}$)	38	128	145	48
b ($\mu S \cdot cm^{-1}$)	624	681	774	781

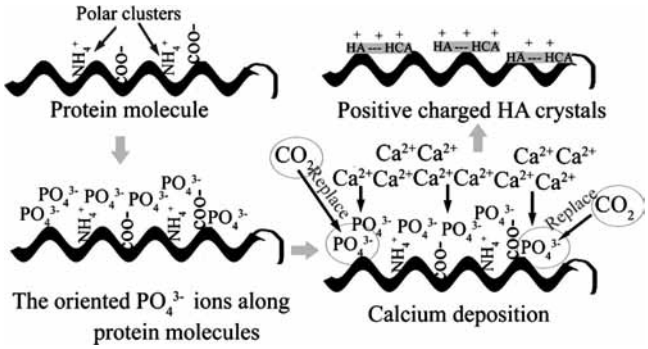

Figure 6. Schematic illustration of the protein-medicated crystallization of HA crystals with positive charges.

nm. The electron diffraction shows strongly focused spots (Figure 4d, see the inset). The irregular diffraction spots indicate the coexistence of a multiphase. The (101) diffraction ring is ascribed to the HA crystal.

3.5. Surface Charge Analysis. Figure 5 shows the electrophoregrams of the powders prepared by the biomimetic route using ovalbumin as biosurfactant. The suspension was prepared by adding 0.05 g of dry powder into 40 mL of distilled water, followed by ultrasonic dispersing for 30 min in an ultrasonic cleaner. Then 0.5 mL of the suspension was placed in an electrophoresis cup, and the movable images of the particles were recorded by the electrophoresis apparatus. The zeta potentials of all the samples are negative, indicating that the particles themselves have superfluous positive electrical charges. According to the FTIR (Figure 3), CO_3^{2-} from air was incorporated with the HA particles, and the replacement of some PO_4^{3-} ions by CO_3^{2-} in the crystal structure may lead to the positive electrical charges.

The electrical conductivities of the powders are shown in Table 3. The electrical conductivity of the distilled water was measured at 5.3 $\mu S \cdot cm^{-1}$. It shows that the electrical conductivity of FB5 reaches a maximum of 145 $\mu S \cdot cm^{-1}$ in aqueous solution, while FB0 and FB7 have the minimum value of 38 $\mu S \cdot cm^{-1}$and 48 $\mu S \cdot cm^{-1}$, respectively. The reason for this is that there are large amounts of organic materials in FB0 which enwrap the particles and hinder their migration in the electric field. The particle size of FB7 is at the micron scale, and most of them will deposit when dispersed in the aqueous solution, resulting in the decrease of the free electrical charges in the suspension. The electrical conductivity of the sodium hydroxide solution (0.033 M) is measured at 790 $\mu S \cdot cm^{-1}$. The addition of FB0 or FB3 decreases the conductivity effectively, while the addition of FB5 or FB7 has almost no influence. This is because FB0 and FB3 contain much more positive charges than FB5 and FB7 (Figure 5), which can adsorb the OH^- ionized from sodium hydroxide to form a stable electrical double layer (EDL), and the charges can be easily stored in either the compact or the diffuse part of the EDL. As a result, the concentration of the free charges in the solution decreases.

According to the analysis above, a schematic illustration is used to depict the protein-medicated crystallization of FB0 (Figure 6). It shows that some PO_4^{3-} ions are substituted by CO_3^{2-} in the crystal resulting in the reduction of the negative charges.

4. Conclusions

The HA/ovalbumin composites were synthesized by means of a biomimetic strategy. XRD and DTA analyses prove that the phase transformation temperature of HA to β-TCP is as low as about 550 °C. The zeta potentials and the electrical conductivities of the powders were studied to characterize the positive electric charges of the particles which were caused by the substitution of CO_3^{2-} for PO_4^{3-} ions. The FTIR and BET analyses show that the ovalbumin has a great effect on the size and the shape of the nanocrystals. Therefore, it can be concluded that the low phase transformation temperature is caused by the cooperative effect of the CO_3^{2-} and the proteins incorporated with the HA crystals. It can also be inferred that the HA/β-TCP polycrystal with different mass ratio can be obtained if given a different heat preservation time above 550 °C.

Acknowledgment

The authors thank the Analytical Center of Shandong Institute of Light Industry, China, for the technological support.

Literature Cited

(1) Neuman, W. F.; Neuman, M. W. *The chemical dynamics of bone mineral*; University of Chicago Press: Chicago, 1958.
(2) Du, C.; Cui, F. Z.; Feng, Q. L.; Zhu, X. D. Tissue response to nano-hydroxyapatite/collagen composite implants in marrow cavity. *J. Biomed. Mater. Res.* **1998**, *42*, 540–548.
(3) Martins, V. C.; Goissis, G.; Ribeiro, A. C.; Marcantonio, E. The Controlled Release of Antibiotic by Hydroxyapatite: Anionic Collagen Composites. *Artif. Organs* **1998**, *22*, 215–221.
(4) Lemosa, A. F.; Rochaa, J. H. G.; Quaresmaa, S. S. F.; Kannana, S; Oktara, F. N.; Agathopoulosa, S.; Ferreiraa, J. M. F. Hydroxyapatite nano-powders produced hydrothermally from nacreous material. *J. Eur. Ceram. Soc.* **2006**, *26*, 3639–3646.
(5) Rusu, V. M.; Ng, C. H.; Wilke, M.; Tiersch, B.; Fratzl, P.; Martin, G. P. Size-controlled hydroxyapatite nanoparticles as self-organized organic-in organic composite materials Source. *Biomaterials* **2005**, *26*, 5414–5426.
(6) Takeuchi, A.; Ohtsuki, C.; Miyazaki, T.; Ogata, S.; Tanihara, M.; Tanaka, H.; Furutani, Y.; Kinoshita, H. Apatite formation on silk fiber in a solution mimicking body fluid. *Key Eng. Mater.* **2003**, *31*, 240–242.
(7) Hutchens, S. A.; Benson, R. S.; Evans, B. R.; O'Neillc, H. M.; Rawn, C. Biomemetic Synthesis of Calicum-Deficient Hydroxyapatite in a Natural Hydrogel. *J. Biomater.* **2006**, *27*, 4661–4670.
(8) Lowenstam, H. A.; Weiner, S. *On Biomineralization*; Oxford University Press: England, 1989.
(9) Li, X. D. *The science and technology of eeg*; Chemical Industry Press: Beijing, China, 2005.
(10) Murugan, R.; Ramakrishna, S. Electrospinning of Nano/Micro Scale Poly(L-lactic-acid) Aligned Fibers and their Potential in tissue engineering. *Cryst. Growth Des.* **2005**, *1*, 111–112.
(11) Zhang, F.; Zhou, Z. H.; Yang, S. P.; Mao, L. H.; Chen, H. M.; Yu, X. B. Hydrothermal synthesis of hydroxyapatite nanorods in the presence of anionic starburst dendrimer. *Mater. Lett.* **2005**, *59*, 1422–1425.
(12) Meejoo, S.; Maneeprakorn, W.; Winotai, P. Phase and thermal stability of nanocrystalline hydroxyapatite prepared via microwave heating. *Thermochim. Acta* **2006**, *1*, 115–120.
(13) Chang, M. C.; Ko, C. C.; Douglas, W. H. Preparation of Hydroxyapatite-gelatin Nanocomposite. *Biomaterials* **2003**, *24*, 2853–2862.
(14) Liu, Y. H.; Liu, P. G. *The application and mechanism of X-ray microanalysis*; Chemical Industry Press: Beijing, 2003.
(15) Zhang, X.; Li, Y. B.; Lv, G. Y.; Zuo, Y.; Mu, Y. H. Thermal and crystallization studies of nano-hydroxyapatite reinforced polyamide 66 biocomposites. *Polym. Degrad. Stab.* **2006**, *91*, 1202–1207.
(16) Roveri, N.; Falini, G.; Sidoti, M. C.; Tampieri, A.; Landi, E.; Sandri, M.; Parm, B. Biologically inspired growth of hydroxyapatite nanocrystals inside. *Mater. Sci. Eng., C* **2003**, *23*, 441–446.
(17) Sato, K.; Kumagai, Y.; Tanaka, J. Apatite formation on organic monolayers in simulated body environment. *J. Biomed. Mater. Res.* **2000**, *50*, 16–20.
(18) Weiner, S.; Bar-Yosef, O. States of preservation of bones from prehistoric sites in the Near east: a survey. *J. Archaeol. Sci.* **1990**, *17*, 187–196.
(19) Surovell, T. A.; Stine, M. C. Standardizing Infra-red Measures of Bone Mineral Crystallinity. *J. Archaeol. Sci.* **2001**, *6*, 633–642.

Received for review January 24, 2008. Accepted October 18, 2008. The authors thank the Natural Science Foundation of China (Grant No. B2052140, B5050470) for the financial support.

JE800058D